Multishot EPI-SSFP in the Heart

Daniel A. Herzka,[1,2*] Peter Kellman,[2] Anthony H. Aletras,[2] Michael A. Guttman,[2] and Elliot R. McVeigh[2]

Refocused steady-state free precession (SSFP), or fast imaging with steady precession (FISP or TrueFISP), has recently proven valuable for cardiac imaging because of its high signal-to-noise ratio (SNR) and excellent blood–myocardium contrast. In this study, various implementations of multiecho SSFP or EPI-SSFP for imaging in the heart are presented. EPI-SSFP has higher scan-time efficiency than single-echo SSFP, as two or more phase-encode lines are acquired per repetition time (TR) at the cost of a modest increase in TR. To minimize TR, a noninterleaved phase-encode order in conjunction with a phased-array ghost elimination (PAGE) technique was employed, removing the need for echo time shifting (ETS). The multishot implementation of EPI-SSFP was used to decrease the breath-hold duration for cine acquisitions or to increase the temporal or spatial resolution for a fixed breath-hold duration. The greatest gain in efficiency was obtained with the use of a three-echo acquisition. Image quality for cardiac cine applications using multishot EPI-SSFP was comparable to that of single-echo SSFP in terms of blood–myocardium contrast and contrast-to-noise ratio (CNR). The PAGE method considerably reduced flow artifacts due to both the inherent ghost suppression and the concomitant reduction in phase-encode blip size. The increased TR of multishot EPI-SSFP led to a reduced specific absorption rate (SAR) for a fixed RF flip angle, and allowed the use of a larger flip angle without increasing the SAR above the FDA-approved limits. Magn Reson Med 47:655–664, 2002. Published 2002 Wiley-Liss, Inc.[†]

Key words: cardiac imaging; fast magnetic resonance imaging; SSFP; FISP; EPI; SENSE; ghost artifacts

Refocused steady-state free precession (SSFP) (1), also known as fast imaging with steady precession (FISP or TrueFISP) (2,3), has proven valuable for in vivo cardiac MRI because of its excellent signal-to-noise ratio (SNR) and myocardium-to-blood contrast-to-noise ratio (CNR) (2,4). In applications such as cine (4,5) acquisitions and real-time (6,7) imaging, among many others, shorter breath-hold times or faster frame rates are highly desirable. Conventional refocused SSFP acquires data for only one line of k-space (i.e., a view) per repetition time (TR) leading to a relatively low data acquisition efficiency (8), as defined by the ratio of data sampling (readout) time (T_s) to TR. Echo-planar imaging (EPI) gains considerable efficiency since the overhead time associated with radiofrequency (RF) excitation and slice selection remains constant while the effective readout time is increased. The

increased efficiency of the combination of EPI and SSFP, even with a short echo train length (ETL), can shorten scan times or increase spatial or temporal resolution with a only a modest increase in TR compared to SSFP acquisitions for which only one view is acquired.

The signal acquired in refocused SSFP is a coherent superposition of the free induction decay (FID), due to the RF pulse immediately preceding the readout, with spin echoes, stimulated echoes, and higher-order echoes from preceding RF pulses (9–14). In this work, the acquisition of one k_y line (i.e., view) is referred to as single-echo SSFP, even though the actual signal is composed of the superposition of the FID and several different echoes. The acquisition of several k_y lines within a single TR with an echoplanar readout is referred to as a multiecho acquisition or EPI-SSFP. This mode of acquisition should not be confused with other types of SSFP acquisitions, such as Fourier acquired steady-state (FAST) and contrast enhanced FAST (CE-FAST) (15), in which the FID and echo components are acquired separately; fast acquisition double echo (FADE) or dual echo in the steady state (DESS) (14,16–18), in which both are acquired independently but simultaneously; and acquisitions in which multiple higher-order echoes are acquired within a single readout (19).

The success of refocused SSFP in cardiac imaging is due to advances in hardware which allow for shorter TRs, leading to reduced effects of field inhomogeneities, chemical shifts, and motion on the steady-state magnetization (5). In particular, short TRs maintain coherence between the various components of the refocused SSFP signal. A consequence of using ultrashort TRs and high flip angles in non-EPI SSFP is a large RF power deposition or specific absorption rate (SAR) (20). The imaging flip angle needs to be limited so the SAR does not exceed FDA-approved levels, thus limiting the achievable contrast between myocardium and blood. EPI-SSFP has an increased TR; thus SAR is reduced for a given flip angle. The limitation in flip angle is relaxed, which increases achievable contrast.

In SSFP, the TR must be minimized to avoid off-resonance artifacts (2). The precession angle of magnetization in the transverse plane during one TR cannot exceed 180° (2,6) to reduce banding or fringe artifacts. This condition implies that TR must be kept less than $\left(\frac{\gamma}{\pi} \left| \Delta B_0 \right| \right)^{-1}$ or $(2 \cdot fs)^{-1}$, where γ is the gyromagnetic ratio, ΔB_0 is the field inhomogeneity, and f_S is the equivalent resonant frequency shift resulting from any local field inhomogeneity or chemical shift. A balance must be sought between increases in TR due to extra readouts and the appearance of banding artifacts due to off-resonance. Reeder et al. (21) report that field inhomogeneities in the myocardium can cause a variation of up to 70 Hz at 1.5 T, placing the upper bound on TR at 7 ms. Similarly, in a study using multiecho FISP for imaging the brain, Heid and Deimling (20) re-

[1]Department of Biomedical Engineering, Johns Hopkins University School of Medicine, Baltimore, Maryland.

[2]Laboratory of Cardiac Energetics, National Institutes of Health, National Heart, Lung and Blood Institute, Bethesda, Maryland.

*Correspondence to: Daniel A. Herzka, Laboratory of Cardiac Energetics, National Institutes of Health, National Heart, Lung and Blood Institute, 10 Center Drive, MSC-1061, Building 10, B1D416, Bethesda, MD 20892-1061. E-mail: herzkad@nih.gov

ported that maintaining a TR of <7 ms at 1.5T is adequate to avoid artifacts in tissues of interest.

Although multiecho FISP has been successfully applied to brain imaging (20), only recently has it been used in the body or the heart. The use of an EPI readout can cause artifacts arising from flow, off-resonance, or other sources of phase or amplitude variation (22–25). Echo time shifting (ETS) (22) can be used to partially mitigate some of the artifacts at the expense of increasing the TR. To eliminate these artifacts without the use of ETS, we used an adaptive phased-array ghost elimination (PAGE) technique (26). This method of ghost cancellation uses a phase-encode acquisition order for which the EPI distortion due to off-resonance and flow has rapid, periodic k-space variation, thereby creating widely spaced ghosts, which are canceled by appropriate phased-array combining. Advantages of this method include a reduction in TR by eliminating echo shifting, cancellation of in-plane flow artifacts, and a reduction of through-plane flow artifacts due to the significant decrease in phase-encode blip size (26).

This work presents the use of multishot EPI-SSFP in segmented cardiac breath-held cine imaging. We demonstrate the benefits of increased efficiency for augmenting the spatial resolution or increasing the number of cardiac phases for a given breath-hold duration, and for decreasing the breath-hold duration for a fixed resolution and number of phases. We characterize the performance of this method in terms of achievable blood–myocardium contrast and compare the performance of ETS and PAGE in terms of the reduction of EPI-induced artifacts.

METHODS

EPI Waveforms

To establish the steady precession condition, there should be minimal phase accrual during one complete TR period. Furthermore, this condition must hold for both stationary and moving spins. This is of particular importance in the heart, where both large flow and motion take place, requiring that gradient waveforms be zeroth- (area) and first- (area · time) moment nulled. Single-echo SSFP achieves this by creating symmetric waveforms that are intrinsically moment nulled in both the readout (G_X) and the slice-selection (G_Z) directions (G_{X1} (Fig. 1)). When EPI-SSFP was used, first-moment nulling in the readout direction over one TR was achieved in several ways. In one implementation of two-echo SSFP, a matched pair of pulses was added after a gradient-recalled echo-train readout waveform ($G_{X2,BIPOLAR}$ (Fig. 1)). The final two lobes were designed to cancel both the zeroth and first moments of the readout waveform. A second implementation used a "flyback" waveform with two positive readout gradients (27) ($G_{X2,FLYBACK}$ (Fig. 1)). Finally, Fig. 1 (G_{X3}) shows a three-echo SSFP implementation. All time-symmetric waveforms are inherently moment nulled. Note that the phase-encoding gradients (G_Y) were only zeroth-moment nulled in all implementations of single- and multiecho EPI-SSFP discussed here. The first moment in the phase-encode direction was reduced with the use of PAGE by minimizing the phase-encode blip size.
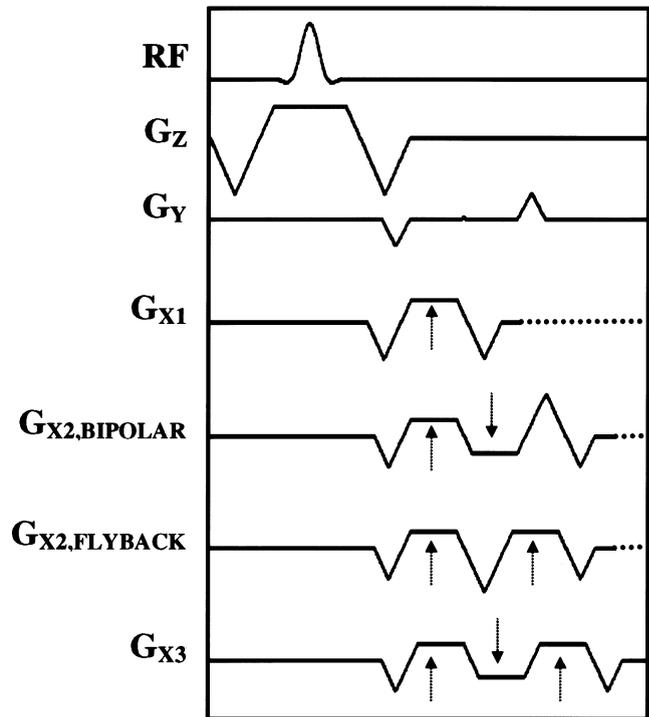

FIG. 1. Pulse sequence used in the implementation of multishot EPI-SSFP including the excitation RF pulse, the slice-selection (G_Z), phase-encoding (G_Y), and readout (G_X) gradients. The first readout waveform (G_{X1}) displays the standard balanced single-echo readout implemented for one-echo SSFP. The second readout waveform corresponds to the bipolar implementation of two-echo SSFP ($G_{X2,BIPOLAR}$), while the third one corresponds to the "flyback" version of two-echo SSFP ($G_{X2,FLYBACK}$). The last readout waveform is that of three-echo SSFP (G_{X3}). All slice-select and readout waveforms are zeroth- and first-moment nulled over TR. The RF transmit and receive phases were alternated to avoid signal cancellation. The phase encoding displayed is that of bipolar two-echo SSFP. Note that although G_Y is not first-moment nulled for any of the implementations displayed here, the use of PAGE greatly reduces the amplitude of the phase-encoding blip. The end of the readout waveforms corresponds to the actual TR of each sequence.

EPI Artifact Suppression

The use of EPI with a short echo train generally results in artifacts primarily from flow and chemical shifts (25). The techniques of ETS and PAGE were implemented separately to mitigate EPI artifacts in multishot EPI-SSFP.

Conventional, multishot EPI with a short echo train uses an interleaved phase-encode acquisition order in conjunction with ETS (22), such that off-resonance distortion is minimized. The resultant TR is increased by almost a full readout period. An alternative method to eliminate ETS was implemented by using a phase-encode order for which the k-space distortion had a rapid periodic variation (26). This caused widely spaced ghosts, spaced D = FOV/ETL, where FOV is the field of view and ETL is the echo train length. The ghosts were then suppressed by means of PAGE, which exploited the difference between multiple coil sensitivities in a manner similar to that used in the sensitivity encoding (SENSE) accelerated imaging method (28).
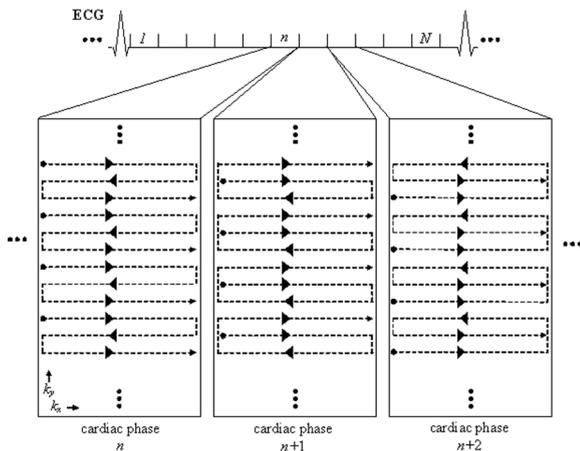
FIG. 2. Phase-encode acquisition order for three-echo SSFP using adaptive phased array ghost elimination (PAGE). The phase-encode acquisition order is varied in a cyclical manner to enable the adaptive calculation of a lower temporal resolution ghost-suppressed image used for computing B_1-maps used in PAGE. In this example, 12 k_y lines are acquired in four RF shots for each cardiac phase (1, ..., n, n + 1, n + 2, ..., N) during each heartbeat. However, the k-space matrix of each cardiac phase is acquired with a slightly varied view-ordering scheme achieved via changes in the phase-encode blip magnitudes. Note that the overall pattern of acquisition is noninterleaved but the ghosts in each image have different phase weighting depending on the acquisition order.

The PAGE method required estimates of the coil sensitivity profiles (B_1-maps). These profiles were calculated adaptively using a time-varying phase-encode order in which the echo order was varied cyclically (Fig. 2). In this manner, lower temporal resolution ghost-suppressed images used for calculating the sensitivities were derived by means of temporal low-pass filtering (26).

Experimental Parameters

All images were acquired with a 1.5 T GE CV/i MRI Scanner (GE, Medical Systems, Wausheka, WI) using an enhanced gradient system with 40 mT · m^{-1} maximum gradient amplitude and 150 T · m^{-1} · s^{-1} slew rate unless otherwise specified. A four-element cardiac phased-array coil was used for all acquisitions. A segmented, gradient-recalled echo sequence with gating capability (29) was modified to run breath-hold multishot EPI-SSFP. To maintain the steady-state condition while gating via the electrocardiogram (ECG), RF pulses were continuously played out while polling for a trigger caused by an R-wave took place. Upon detection of the trigger, data acquisition for the next segment commenced, as described in Ref. 29.

In both humans and phantoms, single-echo SSFP images were acquired for comparison with all implementations of multishot EPI-SSFP using either ETS or PAGE. All images were reconstructed offline. For all acquisitions the number of cardiac phases acquired, breath-hold times, flip angles, and data acquisition efficiency were recorded.

Phantom Studies

The multishot EPI-SSFP technique was tested on stationary phantoms with T_1 and T_2 characteristics similar to those of myocardium and blood. The blood phantom had a T_1 of 804 ms and a T_2 of 283 ms, and the myocardial phantom had a T_1 of 1045 ms and T_2 of 68 ms. Signal intensities (SI) and contrast (C), defined as

$$C = \frac{SI_{Blood} - SI_{Myocardium}}{SI_{Blood}} \qquad [1]$$

were compared for standard single-echo and EPI-SSFP. The following imaging parameters were used: 32 × 24 cm FOV; 10-mm slice thickness; 12 views per cardiac phase per heartbeat (i.e., 12 views per segment), leading to 12, six, or four RF shots for one, two, and three echoes, respectively; 128 × 108 matrix; ±125 kHz receiver bandwidth (RBW); and a 10-segment acquisition with the data from the initial segment discarded to avoid artifacts from the transition into steady state. The flip angle of each acquisition was increased while maintaining the average SAR constant.

The signal-to-noise ratio (SNR) was estimated for images acquired with ETS. Noise images were generated by subtracting a reference image made from the average of all cardiac phases from the original image. The SNR was calculated as the ratio of the mean signal in the region of interest (ROI) to the standard deviation (SD) of the background noise. The PAGE method incurs an SNR penalty that is spatially varying and depends upon a number of factors, including the number of ghosts, number of coils and their sensitivity profiles, and the specific slice geometry. This SNR loss has been characterized and validated previously (26).

Human Studies

This study comprised seven normal, healthy volunteers. The study was approved by the Institutional Review Board of the National Heart, Lung, and Blood Institute. Typical imaging parameters were the same as in the phantom studies except for FOV = 36 × 27 cm; matrix = 128 × 108 or 128 × 144; and 10−13 segment acquisitions, with data from the initial segment discarded to avoid artifacts from the transition into steady state. The flip angle of each acquisition was increased until the average SAR was close to but less than 2.0 W · kg^{-1}. Typically, three short-axis slices and one long-axis slice were acquired per volunteer. To facilitate the comparison of the contrast available with different imaging protocols, the increased efficiency in multishot EPI-SSFP acquisitions was used to acquire extra cardiac phases while maintaining constant breath-hold time and spatial resolution. For each acquisition, myocardium and blood signal intensities were recorded as well as the number of cardiac phases. Breath-hold time reduction was also demonstrated in scans where spatial resolution and number of cardiac phases remained approximately constant. Additionally, higher-resolution images with 256 × 192 matrix and 36 × 27 cm FOV were acquired using 180 T · m^{-1} · s^{-1} slew rates.

The average signal intensities of the myocardium were measured by placing ROIs in sections of myocardium not affected by any flow artifact or ghosting. Blood intensities were measured by placing ROIs in the center of the left ventricular (LV) cavity. The resulting signal intensities and contrast of the last six to eight end-diastolic phases were

Table 1
Averaged Results Obtained From Scans of Seven Normal Volunteers

Acquisition method	EPI ghost suppression method	Flip angle (N = 7)	TR (ms) (N = 7)	Efficiency (T_S/TR) (%) (N = 7)	Increase in cardiac phases (%) (N = 7)	Reduction in breath-hold time (%) (N = 1)
One-echo SSFP	—	58°	3.57 ± 0.14	14 ± 1	—	—
Two-echo SSFP Bipolar	ETS	73°	6.02 ± 0.14	17 ± 1	21.0 ± 5.4	21.4
	PAGE	69°	5.05 ± 0.20	20 ± 1	43.0 ± 2.6	32.2
Two-echo SSFP Flyback	ETS	74°	6.00 ± 0.29	17 ± 1	21.7 ± 6.1	25.0
	PAGE	70°	5.16 ± 0.23	20 ± 2	40.8 ± 1.6	32.1
Three-echo SSFP	ETS	76°	6.28 ± 0.18	24 ± 1	72.2 ± 4.4	53.5
	PAGE	72°	5.32 ± 0.49	29 ± 3	108.3 ± 6.1	53.5

TR varied with slice orientation. Efficiency of data acquisition, defined as the ratio of sampling (readout) time to TR, varies slightly with slice orientation. The increase in TR allowed for increases in imaging flip angle due to reduced SAR constraints. The number of cardiac phases acquired for multishot EPI-SSFP increased relative to one-echo SSFP for scans where spatial resolution and breath-hold times were held constant. Breath-hold time decreased relative to one-echo SSFP for scans in which spatial resolution and number of cardiac phases were held constant. Note that because only discrete values of the views acquired per segment and echotrain length are used, the breath-hold duration did not always decrease.

averaged to obtain an average value for each slice acquired. All slices measured over all seven volunteers were averaged to yield the final results for each method. Spatial locations with predominant flow artifact were not measured, and therefore were not averaged into the final results.

The use of a noise-only ROI to measure noise statistics free of signal (30,31) is well established for measuring the SNR of magnitude images, since it overcomes the difficulty encountered due to nonuniform image intensity. Since the PAGE methods results in spatially varying noise, it was necessary to measure both the mean SI and noise variance in the ROI. In order to measure the local background noise variance in the presence of signal that has intensity variation within the ROI, a high-pass spatial filter technique was employed to suppress low spatial frequency signal components (32). The high-pass spatial filter was designed using a windowed sinc (Kaiser window) with stopband of 0.3 (normalized to the sample frequency) and a 7 × 7 pixel for a smooth transition band in order to reduce filter ringing. The measured filtered noise variance was scaled appropriately to compensate for the equivalent filter bandwidth, which was measured. This method was effective in moderate-size regions such as the LV blood pool. The ROI size for the LV blood pool after image interpolation to 256 × 256 size was on the order of 130 pixels (approximately 32 statistically independent samples). The CNR between the myocardium and blood was measured using the variance measured in the blood pool. For consistency, a mid-septal myocardium ROI location was chosen for all patients. The spatially varying G-factor, which depends on the number of echoes, coil geometry, coil positioning, and slice position, was estimated directly from the complex coil sensitivity profiles that were used for computing the phased-array combining coefficients (28). The G-factor varies considerably over the heart region; therefore minimum, maximum, and mean values were measured.

RESULTS

Efficiency of EPI Waveforms

Table 1 summarizes the increased efficiency gained with multishot EPI-SSFP. The increase in efficiency from the multiecho implementations allowed increased temporal

resolution, as measured by the increase in the number of cardiac phases. When spatial and temporal resolutions were held constant, decreases in breath-hold times as high as 53% were achieved. As expected, the efficiency increased with an increasing number of echoes. Both bipolar and flyback implementations of the two-echo SSFP gave the same increases in efficiency. However, the flyback implementation was sometimes limited by hardware at a few oblique slices for which gradients were unable to sustain the increased switching.

PAGE acquisitions had shorter TRs due primarily to the elimination of ETS. The use of very small phase-encode blips with PAGE further reduced TR. When using ETS, phase-encode blips must have large areas, as the general interleaving scheme requires steps of a half or one-third of k-space for two- and three-echo acquisitions, respectively. These large blips can lead to an increase in echo spacing. Note that the flyback implementation of two-echo SSFP does not suffer this limitation, as there is always enough spacing between readout gradients to fit any necessary blip size. Therefore, the use of PAGE leads to a larger reduction in TR for both the bipolar implementation of two-echo SSFP and the three-echo implementation than it does for the flyback implementation.

Three-echo images acquired with PAGE had an large increase in temporal resolution than those acquired with ETS, as the number of cardiac phases more than doubled with respect to one-echo SSFP in all acquisitions. However, decreases in breath-hold times were the same for both three-echo implementations despite the fact that the efficiencies differed. This was a result of the integer nature of scan parameters such as the number of views acquired per cardiac phase per heartbeat and echo train length.

Image Quality

Figures 3 and 4 display representative images acquired with PAGE and ETS, respectively. Image quality was comparable among all acquisitions. Images acquired with ETS were more likely to suffer signal loss due to susceptibility differences near the heart–lung interface and the posterior vein of the LV as a result of the extended TRs (data not shown) (21,33).

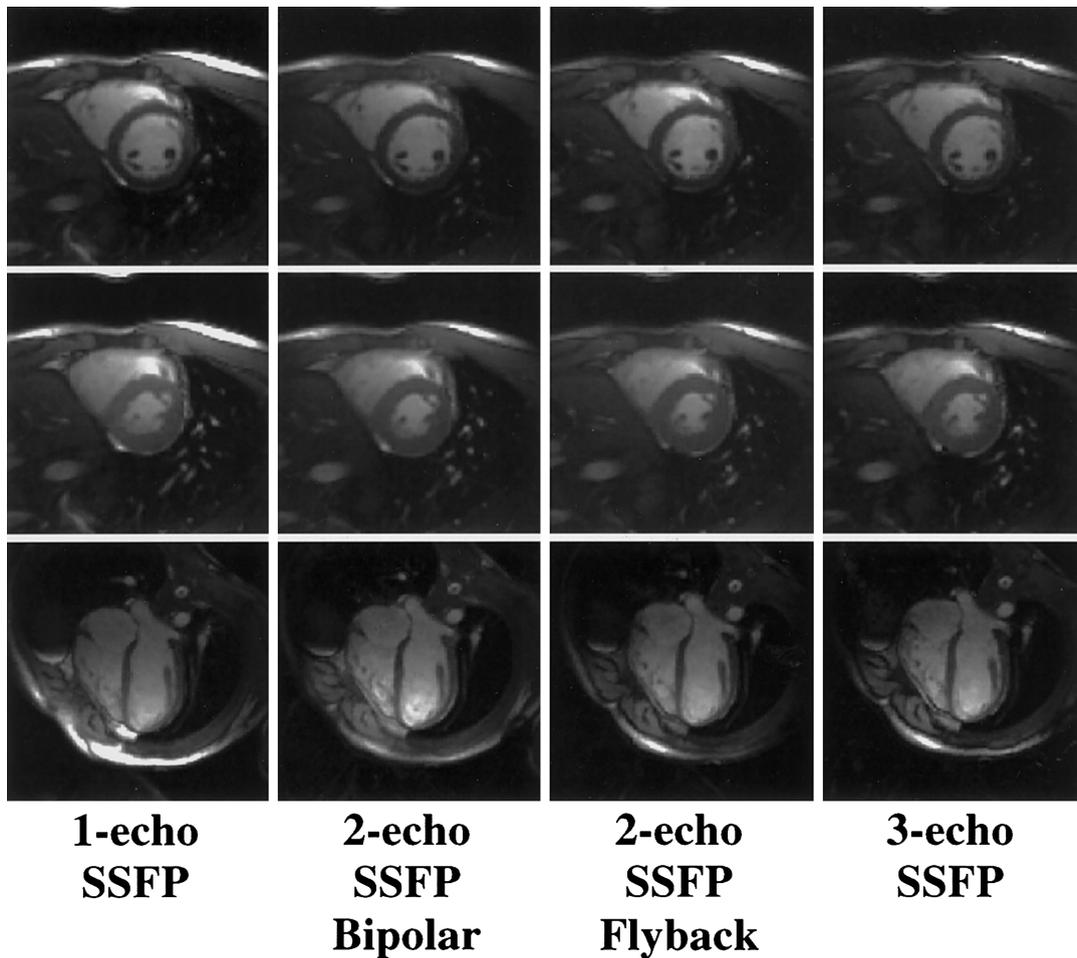**1-echo SSFP**   **2-echo SSFP Bipolar**   **2-echo SSFP Flyback**   **3-echo SSFP**

FIG. 3. Representative one-echo SSFP images and multishot EPI-SSFP images acquired with PAGE. Images acquired with all four methods had similar blood–myocardium contrast. End-diastolic short-axis images (top row) display a susceptibility artifact at the myocardial-lung surface not seen in end-systolic (middle row) images. Long-axis images (bottom row) show fat cancellation resulting from PAGE, particularly in the area of the chest wall.

The SI for the myocardial phantom remained constant for all acquisitions (Fig. 5a). Blood phantom SI was increased for implementations of multishot EPI-SSFP but tended to increase to a greater extent with ETS than with PAGE, as was expected from the use of larger flip angles allowed by the longer TRs of ETS. Figure 5b shows the contrast between the blood and myocardial phantoms. Contrast was maintained with the use of multishot EPI-SSFP. Contrast increased more for ETS acquisitions, as expected by the larger increase in blood phantom SI seen in Fig. 5a. SNR was calculated for the one-echo SSFP and the multishot EPI-SSFP acquisitions using ETS. There was no significant difference in background noise between all multiecho ETS acquisitions and the single-echo acquisition.

The contrast between blood and myocardial tissue was normalized to the appropriate single-echo acquisition for the seven normal volunteers (Fig. 6a). Contrast was maintained with multishot EPI-SSFP. There was no significant difference between any of the multiecho implementations and the single-echo acquisition (paired *t*-test, Bonferroni corrected). ETS images exhibited flow artifacts, particularly at mid-systolic phases. Using PAGE greatly reduced

flow artifacts. Of the 133 slices acquired over all volunteers, nine were rejected due to persistent flow artifact from the following implementations of multiecho EPI-SSFP: four from two-echo bipolar ETS, one from two-echo flyback ETS, one from two-echo bipolar PAGE, and three from three-echo ETS.

The CNR between blood and myocardium was measured for four normal volunteers with images not corrupted by flow artifacts (Fig. 6b). Only the three-echo PAGE acquisition displayed a significant difference with the single-echo acquisition ($P < 0.001$, paired *t*-test, Bonferroni correction), due to a larger *G*-factor-related noise amplification for the three-echo case (see Discussion section). The *G*-factor was measured across the heart ROI for the two- and three-echo cases. The worst-case *G*-factor (hotspot) was approximately 1.3 for two echoes, and was approximately 3.0 for three echoes. The mean loss in CNR for three-echo PAGE corresponded to a *G*-factor of approximately 1.4 in the LV blood pool region. CNR remained relatively constant for all other acquisitions, although those utilizing ETS resulted in higher CNRs, as expected from the use of higher flip angles allowed by longer TRs (2).

1-echo SSFP **2-echo SSFP Bipolar** **2-echo SSFP Flyback** **3-echo SSFP**
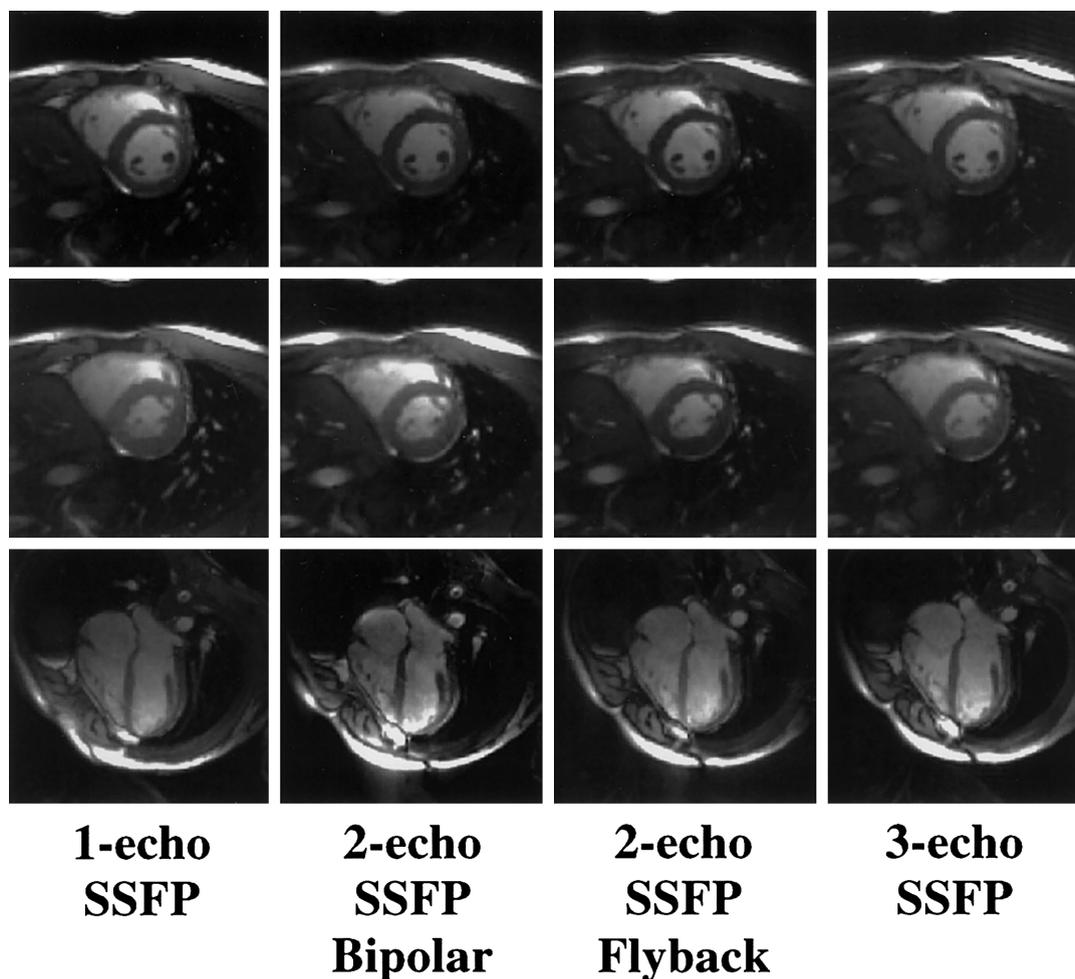
FIG. 4. Representative one-echo SSFP images and multishot EPI-SSFP images acquired with ETS. Top row: end-diastolic short axis; middle row: end-systolic short axis; bottom row: long axis. All multishot EPI-SSFP images acquired with ETS had similar blood–myocardium contrast. Notice that the chemical shift from the fat signal results in blurring.

Figure 7 displays the end-diastolic high-resolution image of a human volunteer acquired with a 256×192 matrix, 36×27 cm rectangular FOV, and $180 \ T \cdot m^{-1} \cdot s^{-1}$ slew rates using two-echo bipolar SSFP with PAGE. Greater detail in the trabeculae and papillary muscles is evident. Off-resonance signal loss artifacts are present due to the longer TR required to obtain the increased number of readout points.

Figure 8b and c shows a typical through-plane artifact found in long-axis images obtained when using two- and three-echo SSFP with ETS. A projection of the bright blood within the aorta creates an artifact that is most prominent during mid-systole. Note that the single-echo SSFP acquisition (Fig. 8a) does not suffer from this artifact. Figure 8d and e displays images obtained using two- and three-echo SSFP and PAGE. Through-plane artifact is greatly reduced with PAGE.

DISCUSSION

Characteristics of EPI Waveforms

Three-echo SSFP displayed the best data acquisition efficiency, since both two-echo implementations required ad-

ditional time to moment null the readout waveform. The bipolar implementation of two-echo SSFP led to shorter TRs than the flyback implementation when used in conjunction with PAGE; the use of smaller phase-encode blips to traverse k-space shortened echo spacing. Blip size had no effect on echo spacing for the flyback implementation.

Flow compensation of the second echo in the bipolar implementation is achieved because both the zeroth and first moments are nulled for even-numbered echoes in bipolar acquisitions (27). It may be possible to shorten the TR of this implementation by using fractional-echo acquisitions, which would further reduce artifacts associated with the use of the echo train by decreasing the echo spacing (22). Note that this waveform is very similar to the three-echo sequence except that the third echo is not sampled, reflecting a loss of efficiency. The second echo in the flyback implementation was not first-moment nulled as it was in the bipolar implementation. However, both echoes had the same zeroth- and first-moment characteristics, which should result in a reduction in artifacts due to step modulations in the phase of the raw data matrix (35). The longer echo spacing in the flyback implementation can exacerbate EPI artifacts such as flow ghosting (22).
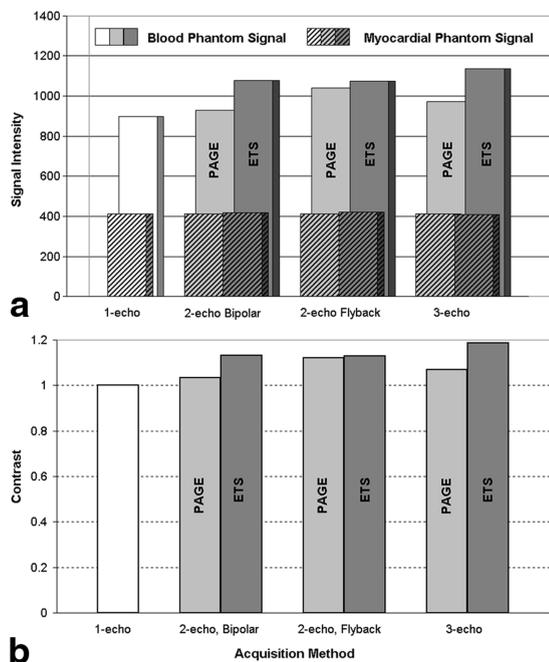
FIG. 5. **a:** Comparison of signal intensities for blood (back, solid) and myocardial phantoms (front, hatched). All methods were able to increase blood phantom signal intensities while the myocardial signal remained constant. **b:** Comparison of contrast, normalized to that of single-echo SSFP. Contrast increased slightly for all implementations of multishot EPI-SSFP, compared to single-echo SSFP. ETS produced slightly higher blood and myocardial SIs than PAGE, leading to slightly better contrast values as expected from the use of higher flip angles allowed by longer TRs.

Image Quality

The longer TRs that resulted from using EPI-SSFP led to a reduction in SAR, which allowed for the use of higher flip angles and yielded slightly increased contrast between myocardium and blood. The increase in contrast was anticipated, as blood SI is expected to increase slightly in the range of flip angles studied while myocardial SI is expected to decrease slightly (2). Hence, higher contrast, as defined in Eq. [1], is expected for higher flip angles.

A limitation of multishot EPI-SSFP was that the increased TR led to greater sensitivity to off-resonance effects. It is expected that TR may be further reduced by pulse sequence design as well as the use of optimized gradient waveforms (34). It should be noted that whereas TRs are extended in multishot EPI-SSFP, they are still relatively short compared to other noncoherent steady-state imaging modalities. In fact, short TRs coupled with the large blip areas (equivalent to half-*k*-space jumps) used in the interleaved view-ordering scheme with ETS contributed to the aortic projection artifact shown in Fig. 8 and discussed next.

The use of multiple echoes involves a loss of signal due to T_2^* decay, particularly during the latter readouts. However, in the case of multishot EPI-SSFP, the TRs are short compared to T_2^*, so little image intensity is lost. Hence, signal intensities for myocardium remain relatively constant regardless of the number of echoes used. The large inflow and outflow effects of blood may contribute to the

increase in blood SI. For example, in Fig. 8 an artifact in which the blood outside of the imaging plane (in the aorta) is projected back onto the image is clearly visible. In this case, blood spins with magnetization in the transverse plane leave the imaging plane at a high velocity, particularly during mid-systole, and traverse the length of the aorta in a short time. Since TR $\ll T_2^*$, these spins continue to contribute signal as they traverse the length of the aorta, outside the imaging plane. In fact, all blood spins leaving the imaging plane should project back onto the imaging plane until T_2^* effects have completely dephased any remaining transverse magnetization. Note that images acquired with PAGE are substantially more resistant to this artifact (Fig. 8d and e) than those obtained with ETS as a result of the sequential phase-encode order (26). The artifact due to out-of-plane coherency is greatly reduced in single-echo SSFP acquisitions (Fig. 8a) that also use a sequential phase-encode order.

EPI Ghost Suppression

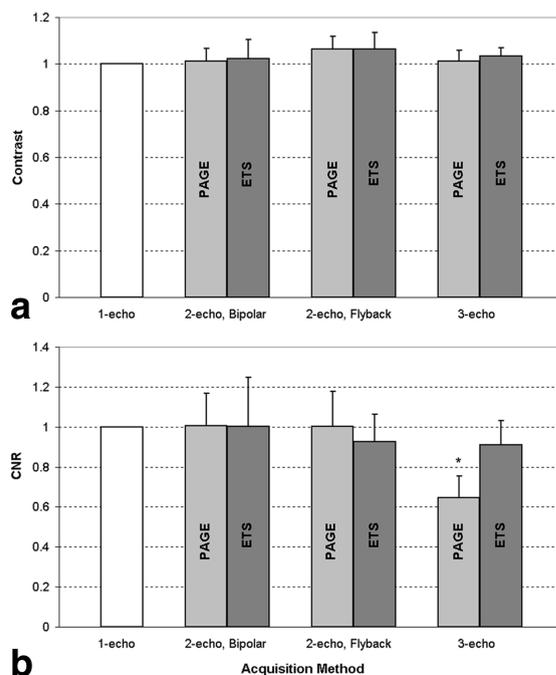The use of PAGE leads to a loss in SNR due to the variance inflation factor inherent in inverse methods. However,

FIG. 6. Average normalized (**a**) contrast ($N = 7$) and (**b**) CNR ($N = 4$) for normal human volunteers. Error bars reflect the SD over all slices averaged. All numbers are normalized to the single-echo SSFP contrast. All implementations of multishot EPI-SSFP slightly increased contrast with respect to one-echo SSFP. There was no significant difference between ETS and PAGE acquisitions with respect to contrast. There was no significant difference in contrast between any of the EPI-SSFP implementations with respect to the single-echo SSFP acquisitions. There was a significant difference in CNR between the three-echo PAGE acquisition and the single-echo SSFP case, as denoted by the asterisk ($P < 0.001$). ETS resulted in slightly higher contrast and CNR values associated with the higher flip angles allowed by longer TRs, although at a lower scan efficiency. PAGE resulted in maintained contrast, as *G*-factor-associated losses canceled the gains of higher flip angles.

FIG. 7. High-resolution (256 × 192, rectangular FOV) end-diastolic image acquired with two-echo bipolar SSFP, PAGE, and 180 T · $m^{-1} \cdot s^{-1}$ slew rates. Higher resolution allows for clearer visualization of the papillary muscle while maintaining excellent blood–myocardium contrast. Note that the susceptibility artifact in the posterior-lateral wall is more prominent due to extended TR.

PAGE benefited from a reduced TR and the resulting minimization of SSFP banding artifacts. The PAGE method allows a reduced phase-encode blip size, which considerably reduced flow artifacts when compared to the ETS method. In general, EPI is sensitive to flow. The interleaved phase-encode acquisition order for ETS gave rise to both in-plane ghosts and through-plane flow artifacts at particular cardiac phases. The PAGE method inherently suppresses in-plane flow ghosts, and has greatly reduced through-plane artifacts due to the greatly reduced phase-encode blip size required by the noninterleaved phase-encode acquisition order scheme (Fig. 2). Furthermore, as scanners with a larger number of coils (e.g., eight coils) become available, the acquisition of images using PAGE with four or five echoes may become possible.

Comparison of EPI-SSFP With PAGE and SENSE Accelerated Imaging

The PAGE method is used to suppress ghosts introduced by the use of multishot EPI with a sequential phase-encode acquisition order. Similarly, SENSE, as used in accelerated imaging, cancels the alias ghosts that result from intentional k-space undersampling. Both PAGE and SENSE have noise variance inflation due to the ill conditioning of the inverse solution used. As described here, the application of PAGE to multishot EPI increases scan efficiency by acquiring multiple lines of k-space per shot without the need for ETS, whereas in the conventional application of SENSE imaging, the acceleration is strictly due to the undersampling. It is worth comparing the scan-time efficiency, SNR, and image quality of these methods to better understand and exploit their potential uses.

In the case of PAGE applied to three-echo SSFP, the scan time is $TR_3 \cdot N_y/3$, and for SENSE with acceleration rate $(R) = 3$, the scan time is $TR_1 \cdot N_y/3$, where N_y is the number of phase-encode lines in the final reconstructed image, TR_1 is the TR for a single readout SSFP acquisition, and TR_3 is the TR corresponding to a three-echo EPI-SSFP acquisition $(TR_3 > TR_1)$. Therefore, the relative scan-time efficiency is the ratio of the TRs, TR_3/TR_1. For the experimental parameters used in this work, for double-oblique slices, SENSE with $R = 3$ is approximately 40% faster $(TR_3/TR_1 \approx 1.4)$. It is expected that further optimization of multiecho SSFP (by methods described in Ref. 34) will reduce the TR; therefore, the $R = 3$ SENSE acquisition would only be 25% faster $(TR_3 /TR_1 \approx 1.25)$. SNR for both of these methods follows the equation $SNR \propto 1/(G \cdot \sqrt{R})$, where G is the noise inflation factor and R is the acceleration rate for SENSE (28); for the PAGE method $R = 1$. Both methods suffer the same noise inflation factor, G; however, the SENSE-accelerated method incurs an additional $\sqrt{R}$ loss in SNR due to undersampling. Therefore, in the $R = 3$ example, SENSE is approximately 25–40% faster, yet it has a loss of 70% in SNR when compared to the PAGE method applied to a three-echo acquisition. In short, the PAGE method as applied to a three-echo acquisition has higher SNR efficiency, defined as SNR per root-time, than an $R = 3$ SENSE acquisition as long as $3 \cdot TR_1 > TR_3$. Equivalently, there is an increase in SNR efficiency with the multiecho acquisition that is not obtained with the SENSE acquisition.

Comparing three-echo PAGE with $R = 2$ SENSE is slightly more complicated, as the G factors will differ between these two cases. The $R = 2$ SENSE method is slower than the three-echo PAGE method (scan times = $TR_1 \cdot N_y/2$ and $TR_3 \cdot N_y/3$, respectively) and has a 40% loss in SNR due to undersampling, but has a considerably improved G-factor using the current four-element cardiac array. In terms of SNR efficiency, the multiecho acquisition is more efficient as long as $(G_2/G_3)^2 \cdot 3 \cdot TR_1 > TR_3$, where G_2 and G_3 are the G-factors associated with $R = 2$ and $R = 3$ acceleration rates, respectively. The ratio of the G-factors becomes the dominant factor in determining the best SNR efficiency. With the current four-coil cardiac array, a three-echo PAGE acquisition has slightly lower SNR efficiency than $R = 2$ SENSE for worst-case locations (i.e., G-factor hotspots). Newer systems with eight coils have substantially improved G-factors, with worst-case G_3 estimated to be 1.3 in the heart.

The flow artifacts for the SENSE single-echo SSFP method, which uses a sequential phase-encode order, should be comparable to the multiecho PAGE method, since the flow artifacts with single-echo SSFP and three-echo SSFP using PAGE (both of which use a sequential phase-encode order) are comparable. The SENSE method was not evaluated experimentally in this study.

CONCLUSIONS

Several implementations of multiecho SSFP were tested and compared in a multishot EPI sequence. All implementations maintained blood–myocardium contrast when compared to the standard refocused SSFP acquisition with only one readout per TR. Both two- and three-echo SSFP
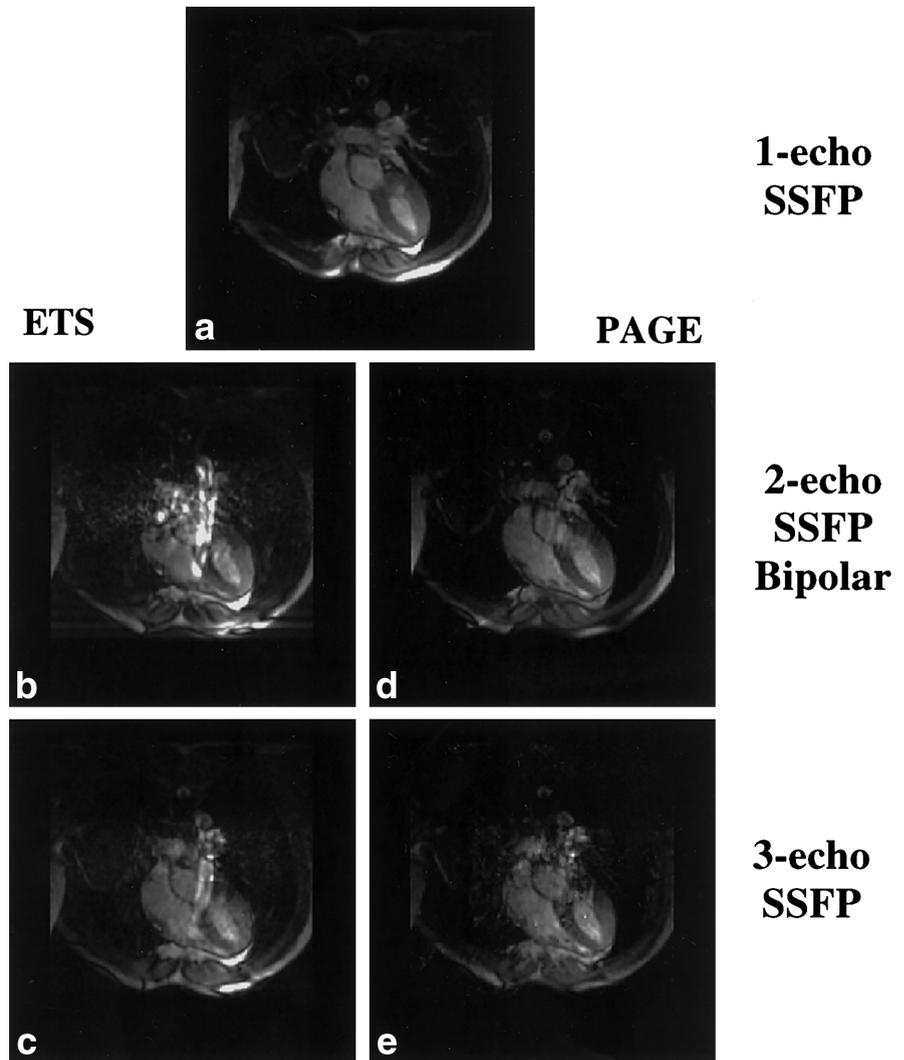
FIG. 8. Aortic flow artifact visible in long-axis images of the heart. The (**a**) single-echo SSFP image does not exhibit flow artifact; however, ETS images for (**b**) two- and (**c**) three-echo SSFP (left column) are considerably more susceptible to this artifact than (**d** and **e**) PAGE-reconstructed images (right column). Different phase-encode ordering schemes led to drastic differences in phase-encode blip sizes between the ETS and PAGE acquisitions, and therefore to differences in flow artifacts.

acquisitions increased data acquisition efficiency, but better results were obtained with the three-echo acquisition. Further optimization of the multishot EPI-SSFP sequence, via the use of faster gradients or optimized gradient waveforms, will continue to increase the gain in efficiency available with this technique.

The increases in efficiency achieved with the various implementations led to a more than doubling of the number of cardiac phases acquired at constant breath-hold time or, equivalently, a reduction in breath-hold time of over 50%. These gains were achieved while maintaining image quality as well as blood–myocardium contrast, and allowed for either the decrease in SAR or an increase in the imaging flip angle.

To correct for EPI-induced artifacts, phased array ghost elimination, PAGE, was implemented, which resulted in shorter TRs primarily by removing the need for ETS. However, because an inversion process similar to that of SENSE-accelerated imaging was used, noise variance inflation and the associated decrease in SNR were observed. This was of particular importance in the three-echo acquisitions, wherein noise variance inflation and gain in acquisition efficiency were highest. The increase in background noise further led to a reduction in blood–myocardium CNR, although given the excellent SNR in refocused SSFP images in general, this is an acceptable loss for the large increase in efficiency obtained with the technique. The implementation of multishot EPI-SSFP in systems with a larger number of coils will further reduce SNR penalties associated with a three-echo acquisition, making multiecho SSFP in combination with PAGE an excellent alternative for faster cardiac imaging.

This study demonstrated that the increased efficiency of multishot EPI-SSFP leads directly to shorter scan times, higher spatial resolution (more views), and higher temporal resolution (more cardiac phases). This is of particular importance in cardiac imaging, in which shorter breath-hold times can lead to more comfortable scans for patients or to more spatial locations acquired within each breath-hold. Furthermore, applications such as real-time imaging, wherein higher efficiencies lead to higher frame rates, can readily benefit from multishot EPI-SSFP. The combination of multishot EPI-SSFP with a phased array ghost elimination technique removed the need for echo time shifting, decreased TR, and reduced the appearance of artifacts related to flow.

ACKNOWLEDGMENTS

REFERENCES

1. Carr HY. Steady-state free precession in nuclear magnetic resonance. Phys Rev 1958;112:1693–1701.
2. Sekihara K. Steady-state magnetization in rapid NMR imaging using small flip angles and short repetition intervals. IEEE Trans Med Imaging 1987;6:157–164.
3. Oppelt A, Graumann R, Fischer H, Hartl W, Schajor W. Fisp—a new fast MRI sequence. Electromedica 1986;54:15–18.
4. Carr J, Simonetti O, Kroeker R, Bundy J, Pereles S, Finn JP. Segmented TrueFISP—an improved technique for cine MR angiography. In: Proceedings of the 8th Annual Meeting of ISMRM, Denver, 2000. p 199.
5. Bundy J, Simonetti O, Laub G, Finn JP. Segmented TrueFISP cine imaging of the heart. In: Proceedings of the 7th Annual Meeting of ISMRM, Philadelphia, 1999. p 1282.
6. Heid O. True FISP cardiac fluoroscopy. In: Proceedings of the 5th Annual Meeting of ISMRM, Vancouver, Canada, 1997. p 320.
7. Fang W, Pereles FS, Bundy J, Kim R, Wu E, Simonetti O, Finn P. Evaluating left ventricular function using real-time TrueFISP: a comparison with conventional MR imaging. In: Proceedings of the 8th Annual Meeting of ISMRM, Denver, 2000. p 308.
8. Reeder SB, McVeigh ER. The effect of high performance gradients on fast gradient echo imaging. Magn Reson Med 1994; 32:612–621.
9. Zur Y, Stokar S, Bendel P. An analysis of fast imaging sequences with steady-state transverse magnetization refocusing. Magn Reson Med 1988;6:175–193.
10. Gyngell ML. The steady-state signals in short-repetition-time sequences. J Magn Reson 1989;81:474–483.
11. Kim DJ, Cho ZH. Analysis of the higher-order echoes in SSFP. Magn Reson Med 1991;19:20–30.
12. Petersson JS, Christoffersson J-O. A multidimensional partition analysis of SSFP image pulse sequences. Magn Reson Imaging 1997;15:451–467.
13. Duyn JF. Steady state effects in fast gradient echo magnetic resonance imaging. Magn Reson Med 1997;37:559–568.
14. Lee SY, Cho ZH. Fast SSFP gradient echo sequence for the simultaneous acquisitions of FID and echo signals. Magn Reson Med 1988;8:142–150.
15. Gyngell ML. The application of steady-state free precession in rapid 2DFT NMR imaging: FAST and CE-FAST sequences. Magn Reson Imaging 1988;6:415–419.
16. Redpath TW, Jones RA. FADE—a new fast imaging sequence. Magn Reson Med 1988;6:224–234.
17. Bruder H, Fischer H, Graumann R, Deimling M. A new steady-state imaging sequence for simultaneous acquisition of two MR images with clearly different contrasts. Magn Reson Med 1988;7:35–42.
18. Hardy PA, Recht MP, Piriano D, Thomasson, D. Optimization of a dual echo in the steady state (DESS) free precession sequence for imaging cartilage. J Magn Reson Imaging 1996;6:329–335.
19. Mizumoto CT, Yoshitome E. Multiple-echo SSFP sequences. Magn Reson Med 1991;18:244–250.
20. Heid O, Deimling M. Multi-echo true FISP imaging. In: Proceedings of the 3rd Annual Meeting of ISMRM, Nice, France, 1995. p 481.
21. Reeder SB, Faranesh AZ, Boxerman JL, McVeigh ER. *In vivo* measurement of T_2^* and field homogeneity maps in the human heart at 1.5 T. Magn Reson Med 1998;39:989–998.
22. Feinberg DA, Oshio K. Phase errors in multi-shot echo planar imaging. Magn Reson Med 1994;32:535–539.
23. Butts BS, Riederer SJ. Analysis of flow effects in echo-planar imaging. J Magn Reson Imaging 1992;2:285–293.
24. Farzaneh F, Riederer SJ, Pelc NJ. Analysis of T2 limitations and off-resonance effects on spatial resolution and artifacts in echo-planar imaging. Magn Reson Med 1990;14:123–139.
25. Reeder SB, Atalar E, Bolster Jr BD, McVeigh ER. Multi-echo segmented *k*-space imaging: an optimized hybrid sequence for ultrafast cardiac imaging. Magn Reson Med 1997;38:429–439.
26. Kellman P, McVeigh ER. Ghost artifact cancellation using phased array processing. Magn Reson Med 2001;46:335–343.
27. Feinberg DA. Echo planar imaging with asymmetric gradient modulation and inner volume excitation. Magn Reson Med 1990;13:162–169.
28. Pruessmann KP, Weiger M, Scheidegger MB, Boesiger P. SENSE: sensitivity encoding for fast MRI. Magn Reson Med 1999;42:952–962.
29. Epstein FH, Wolff SD, Arai AE. Segmented *k*-space fast cardiac imaging using an echo-train readout. Magn Reson Med 1999;41:609–613.
30. Henkelman RM. Measurement of signal intensities in the presence of noise in MR images [erratum published in Med Phys 1986;13:544]. Med Phys 1985;12:232–233.
31. Constantinides CD, Atalar E, McVeigh ER. Signal-to-noise measurements in magnitude images from NMR phased arrays. Magn Reson Med 1997;38:852–857.
32. De Wilde JP, Lunt JA, Straughan K. Information in magnetic resonance images: evaluation of signal, noise and contrast. Med Biol Eng Comput 1997;35:259–265.
33. Atalay MK, Poncelet BP, Kantor HL, Brady TJ, Weisskoff RM. Cardiac susceptibility artifacts arising from the heart-lung interface. Magn Reson Med 2001;41:341–345.
34. Atalar E, McVeigh ER. Minimization of dead-periods in MRI pulse sequences for oblique imaging planes. Magn Reson Med 1994;32:773–778.
35. Duerk JL, Simonetti OP. Theoretical aspects of motion sensitivity and compensation in echo-planar imaging. J Magn Reson Imaging 1991;1:643–650.